Computational Parametric Studies Investigating the Global Hemodynamic Effects of Applied Apical Torsion for Cardiac Assist

Elaine Soohoo [ORCID],[1] Lewis K. Waldman,[2] and Dennis R. Trumble[3]

[1]Scott Hall 4N003, Carnegie Mellon University, 5000 Forbes Avenue, Pittsburgh, PA 15213, USA; [2]Insilicomed, Inc., 7825 Fay Ave Suite 200, La Jolla, CA 92037, USA; and [3]Scott Hall 4N115, Carnegie Mellon University, 5000 Forbes Avenue, Pittsburgh, PA 15213, USA

Associate Editor Estefanía Peña oversaw the review of this article.

Abstract—Healthy hearts have an inherent twisting motion that is caused by large changes in muscle fiber orientation across the myocardial wall and is believed to help lower wall stress and increase cardiac output. It was demonstrated that applied apical torsion (AAT) of the heart could potentially treat congestive heart failure (CHF) by improving hemodynamic function. We report the results of parametric computational experiments where the effects of using a torsional ventricular assist device (tVAD) to treat CHF were examined using a patient-specific bi-ventricular computational model. We examined the effects on global hemodynamics as the device coverage area (CA) and applied rotation angle (ARA) were varied to determine ideal tVAD design parameters. When compared to a baseline, pretreatment CHF model, increases in ARA resulted in moderate to substantial increases in ejection fraction (EF), peak systolic pressures (PSP) and stroke work (SW) with concomitant decreases in end-systolic volumes (ESV). Increases in device CA resulted in increased hemodynamic function. The simulation representing the most aggressive level of cardiac assist yielded significant increases in left ventricular EF and SW, 49 and 72% respectively. Results with this more realistic computational model reinforce previous studies that have demonstrated the potential of AAT for cardiac assist.

Keywords—Congestive heart failure, Ventricular assist device, Computational modeling.

ABBREVIATIONS

AAT	Applied apical torsion
CHF	Congestive heart failure
CA	Coverage area
ARA	Applied rotation angle
HF	Heart failure
tVAD	Torsional ventricular assist device
EF	Ejection fraction
PSP	Peak systolic pressures
SW	Stroke work
ESV	End systolic volume
CO	Cardiac output
LV	Left ventricle
RV	Right ventricle
PV	Pressure–Volume

Address correspondence to Elaine Soohoo, Scott Hall 4N003, Carnegie Mellon University, 5000 Forbes Avenue, Pittsburgh, PA 15213, USA. Electronic mail: esoohoo@andrew.cmu.edu, lwaldman@san.rr.com, dtrumble@andrew.cmu.edu

INTRODUCTION

Despite decades of research and hundreds of millions of dollars aimed at developing effective treatments for congestive heart failure (CHF) this disease remains one of the leading causes of death in the world today, affecting over 5 million people in the United States alone and contributing to 1 in every 9 deaths nationwide.[3] Patients suffering from CHF have hearts that are unable to pump blood at levels sufficient to meet bodily requirements, which can lead to a variety of symptoms, including fatigue, shortness of breath, chest pain, swelling of the legs and feet, mental confusion/memory loss, and organ failure. Factors contributing to the development of CHF in adults vary widely and include irregular heartbeat (arrhythmia), cardiomyopathy, valve disease, coronary artery obstruction, and high blood pressure. These conditions damage the cardiac muscle over time, leading to increased stresses in the heart walls, decreased pumping efficiency, and significant reductions in CO.

When faced with choosing a treatment strategy to combat this disease, CHF patients currently have three main options: pharmacological management, blood pump therapy, and total heart replacement (cardiac transplantation).[26,27] The problem is that none of these interventions can be considered 'curative' and all have serious limitations with regard to long-term effectiveness and overall quality of life. Pharmacological interventions can help restore and manage heart function in the short term and are typically used to relieve the symptoms associated with CHF, but for most patients these therapies are unable to fully restore and support normal heart function over the long term. Cardiac assist devices can be an effective alternative for end stage CHF patients by restoring normal blood flow to the body and helping the heart to pump more efficiently by unloading the ventricles. However, long-term use of these devices are associated with life-threatening complications due to driveline infections, bleeding and thromboembolic events. Currently, total heart transplantation is considered the most effective treatment for end stage CHF. However, the high costs of the procedure, the serious side effects associated with long-term use of immunosuppressive drugs, and the extremely limited pool of donor hearts eliminates this as a viable treatment option for most patients.

The goal of this work is to develop a mechanical means to support the failing heart over the long term while eliminating the risk of thromboembolic complications common to all cardiac assist devices currently on the market. Specifically, our aim is to address the longstanding problem of blood activation due to blood-contacting surfaces by developing a torsion-based ventricular assist device (tVAD) that avoids blood contact altogether. This approach to cardiac support was originally inspired by the contractile mechanics of healthy human hearts, which produce a "wringing" motion during systole that allows the ventricles to empty more completely and reduces transmural stresses acting on the heart walls. This characteristic twisting motion is frequently altered (or missing altogether) in diseased hearts, which is thought to result in accelerated disease progression, lowered cardiac efficiency and decreased global function. Therefore, it is reasonable to hypothesize that restoring this wringing motion to the beating heart may help return the heart to healthy hemodynamic function. Previous studies, done separately by Trumble et al. and Roche et al.[23,24,28] have demonstrated through computational, in vitro, and in vivo experiments that this applied wringing motion has the potential to return cardiac hemodynamics towards a healthier state.

To test this hypothesis we first developed a multiscale prolate model of a failing LV and simulated the effects of AAT via computational means, the results of which were subsequently validated experimentally in a pig model. Findings from these preliminary studies were extremely encouraging but not conclusive owing to the idealized nature of the heart model used and the limited number of torsion modes examined.[28]

Here we report results from a second set of computational experiments wherein varying degrees of rotation and apical CAs were imposed on a more accurate and complete representation of the failing human heart. These studies were designed to determine the best combination of ARA and CA to be used in follow-on parametric studies examining the effects of rotation speed and timing on global ventricular function. Ultimately, findings from these computational parametric studies will be used as a whole to establish design specifications for a fully functional tVAD prototype suitable for in vivo testing.

MATERIALS AND METHODS

The effects of the tVAD on cardiovascular hemodynamics were evaluated by varying the parameters of ARA and the effective device CA adjacent to the cardiac apex on which the rotation is applied. In all studies, a high-order, biventricular model of the beating heart was employed using Continuity Pro computational modeling software (Insilicomed, Inc., La Jolla, CA). The software, simulation techniques and workflows are based on the research of the Cardiac Mechanics Research Group in the Bioengineering Department at University of California, San Diego. The heart model was selected from a cohort of 13 patient-specific computational models of HF in our database. Because of the wide variation of cardiac geometries of these dilated cardiomyopathy patients, a model was chosen in the mid-range of the enlarged hearts. Since these are follow-on studies to simplified single ventricle modeling, a biventricular model in the mid-range of dilated HF models was designed to be generic in nature. Its dimensions are provided in Appendix 1, along with left and right ventricular cavity volumes for some of the configurations used in these studies.

The biventricular models in the database were developed using medical imaging and other clinical measurements obtained from patients with dyssynchronous HF, who were indicated for cardiac resynchronization therapy (CRT). They were correlated with the available clinical data[14,16] to match the geometry, passive, nonlinear material properties, active state and circulatory properties of individual patients. The workflow and correlation methods are delineated in detail.[16]

However, it was necessary to make modifications to the original baseline model to make it useful for the parametric studies described here. Most of the patients in the database had left bundle branch block (LBBB) and typical baseline EFs averaging about 27–28%. However, patients indicated for ventricular assist are likely to have even lower EFs and may not be dyssynchronous in more than half of the cases. Therefore, a number of additional modifications to the original baseline model were made, described in detail in Appendix 1. In brief, a baseline EF of about 20% was selected, and the baseline model was modified to achieve it. An extensive review of the literature on circulatory properties was performed to understand the range of circulatory impedance, resistance and compliance associated with HF in the systemic and pulmonic circulations.[4–6,8–10,12,14,17–22,25,29]

Moreover, a variation in activation times was not included. The direction of myofibers varied throughout the ventricles and was based on DT-MRI of a cadaver heart. The main correlation with clinical data for this patient involved the dilated geometry of the heart, which was fitted using B-mode echocardiographic views. In the CRT studies, baseline biventricular models are fitted to the echo views in prolate spheroidal coordinates. Then, they are transformed to rectangular Cartesian coordinates. However, the shape and dimensions of a given model are independent of the coordinate system due to the tri-cubic, Hermite interpolation scheme. In these studies, the original prolate coordinates are kept due to the ease with which moving boundary problems can be performed utilizing the theta coordinates of rotated nodes alone in this coordinate system (λ, μ, θ). Node rotations are handled using a Python script that interacts with the boundary conditions embedded in the computational model to perform the moving boundary problem concurrently with inherent cardiac function. In these studies, as in the simplified analysis performed previously, a sinusoidal upswing is applied to create the rotation during isovolumic contraction and most of ejection. Then, a slow, linear return rotation is applied for the remainder of the cardiac cycle, as detailed subsequently. The boundary conditions of the model are provided in Appendix 1.

In these studies, the baseline HF model was inflated yielding an initial configuration for subsequent modeling. Using this model, active state was incorporated along with dual, closed-loop circulatory models as described in more detail in Appendix 1, in which the parameters of the dynamic cellular model and circulatory models are provided. For the rotation studies, we examined the effects of varying the ARA for each of three fixed CAs. To do so, moving boundary conditions were applied on select finite element nodes at and basal to the apex, simulating a tVAD that covers 12.5, 18.2 and 24% of the longitudinal distance from the apex towards the base of the ventricles.

Two versions of the same finite element model were employed to make overall solution times for the parametric studies more practical. The models are identical in every way, except for the amount of refinement. For the smallest and largest CAs, an 80-element tri-cubic Hermite model was employed. For the intermediate CA, the 96-element model with one additional circumference midway between smallest and largest CAs was used (Fig. 1). The method of refinement is detailed in Appendix 1. Both 80 and 96-element models were inflated to 1.5 kPa. After incorporating dynamic and circulatory properties (Appendix 1), the models were run till steady-state cardiac cycles were obtained; the results from the two models are identical. These studies provide the baseline HF hemodynamics presented in the results section. In subsequent ARA studies, a counterclockwise rotation, in the same direction but much larger than the natural torsion as viewed from the apex, was applied to the apical region of the ventricles for 187.5 ms during isovolumic contraction and most of ejection. Then, the region was rotated back during the remainder of each 750 ms cardiac cycle (80 beats per minute). Each simulation was run for 10 cardiac cycles or until stroke volumes from each ventricle differed by 5% or less ensuring fully converged solutions, i.e., repeating PV-loops. Subsequently, the last cardiac cycle was used for analysis of global hemodynamics.

For each of the three CAs, simulations were performed in which results from four maximum ARA (45°, 55°, 65°, and 75°) were compared to those of a baseline HF model (NoVAD) simulating a diseased heart pretreatment and a static tVAD support model (0°) where no active cardiac assist is provided. Although the baseline, 0° and 45° simulations behaved well with time steps of 1 ms, large maximum rotations required a time step of 0.5 ms for all three CAs. Moreover, efforts to increase either the CA, as mentioned, or ARA above 75° also led to diverging solutions. Potential reasons for these phenomena are discussed in the last section and Appendix 1.

Additional simulations were performed for the large coverage case due to the findings that are presented in the results. Substantial improvements in cardiac function estimated for this case with maximum rotations of 65° and 75° indicated that this range of angles justified further study. Two more cases were simulated at equal angle increments, i.e., 68.33° and 71.67°.

In Fig. 2, the deformed model is shown at peak pressure for the large coverage case undergoing an ARA of 55°. The epicardial surface has been rendered at low resolution to illustrate substantial displacement of much of the surface, as is evident from the visible mesh longitude in each view and neighboring epicardium.
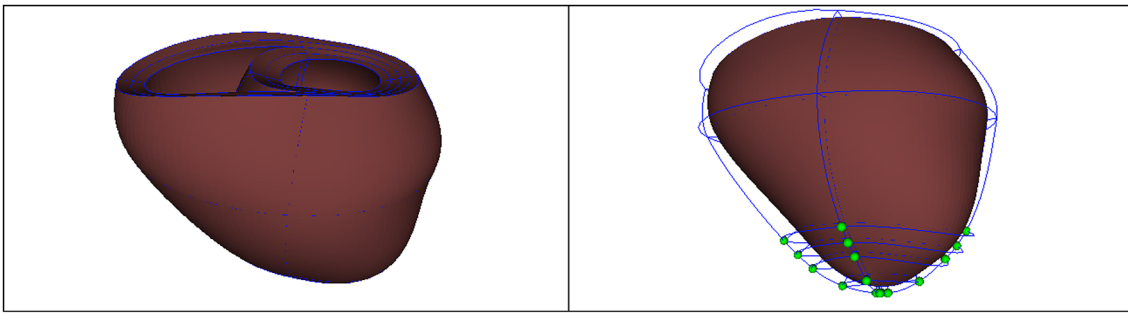
FIGURE 1. Biventricular heart failure model in the no load state; (left) model with epicardial and basal surfaces rendered; (right) model with endocardial surface of outer layer rendered along with all nodes that undergo applied rotation along with corresponding circumferences (posterior set of 5 nodes not visible). *Note* all 20 nodes are rotated for the large coverage runs; 16 nodes are rotated for the intermediate coverage runs, i.e., the most basal set of nodes shown on the upper circumference of the coverage region is excluded; 12 nodes are rotated for the small coverage runs, i.e., the two most basal sets of nodes are excluded.
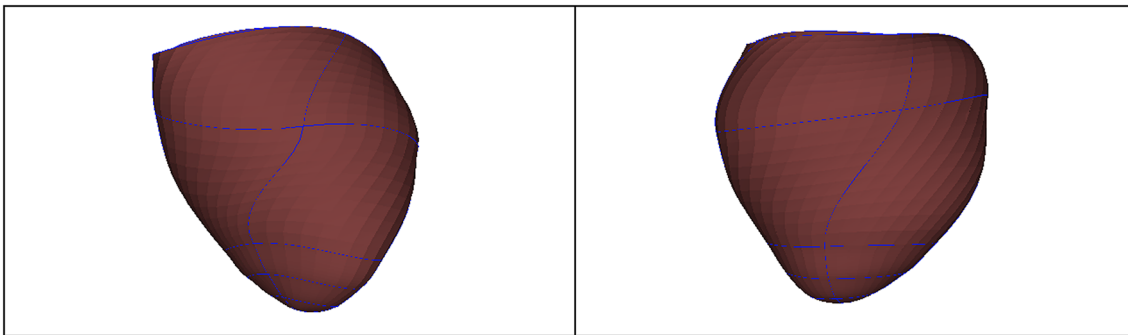

FIGURE 2. To illustrate the applied rotation in the case of large coverage, the deformed state of the model with large coverage and a maximum applied rotation of 55° is shown in two views; the epicardial surface has been rendered in low resolution to show how it is being displaced at the time of peak pressure during the cardiac cycle; in this case, this time preceded maximum rotation by 7 ms; left panel is an anterior view; right panel is a posterior view.

To quantify the effects of CA and maximum rotation, the hemodynamic parameters of EF, PSP, ESV and SW were calculated. The values of EF, PSP, and ESV were computed in Matlab R2015A (MathWorks, Inc., Natick, MA, USA) from the hemodynamics output during the final cardiac cycle of each simulation. To calculate SW, Image J (U.S. National Institutes of Health, Bethesda, Maryland, USA) was used to measure the area circumscribed by the PV-loop of that cardiac cycle. This method is considerably easier than using MatLab for the same purpose and just as accurate (Appendix 1). In the case of the largest rotation and largest CA, results from Matlab were compared with Image J—9171 and 9145 mmHg mL, respectively—and were virtually identical with a difference of less than 0.3%.

RESULTS

Here we report results obtained by varying both the ARA and device CA in simulated beating hearts to quantify their potential effects on global cardiac hemodynamics. Based on these simulations we found that the more aggressive rotations and higher CAs resulted in significant positive changes in key functional parameters, which suggest that torsion therapy may be a viable means to support the failing heart (Tables 1 and 2).

Overall, changes in rotation angle proved to be the more dominant factor in determining the effectiveness of this approach. Specifically, as the angle of apical rotation was increased beyond 45° in the computer model, clinically significant changes were observed in ventricular EF, PSP, ESV and SW when compared to the baseline HF model. EF improved proportionally with torsion applied in the 45°–75° range, suggesting that CO can be augmented to a significant degree with torsion therapy (Fig. 3). PSP also increased proportionally with torsion angle demonstrating that the rotation applied by the tVAD is helping the heart to empty more completely by mechanically displacing more blood (Fig. 4). Likewise, SW was found to increase dramatically with AAT, demonstrating that tVAD assisted ventricles are able to eject larger volumes of blood under

TABLE 1. Resulting left ventricular hemodynamics from rotation studies for the baseline heart failure case (No VAD), 12.5, 18.2, and 24% device coverage areas.

	Angle (°)	EF (%)	PSP (mmHg)	ESV (mL)	SW (mmHg mL)
No VAD		20.33	122.60	200.30	5321
12.5% coverage	0	20.67	124.19	197.68	5503
	45	21.37	124.39	191.12	5624
	55	21.86	124.73	186.04	5800
	65	22.57	126.71	180.14	6010
	75	23.67	130.81	172.69	6236
18.2% coverage	0	20.70	124.34	197.70	5615
	45	21.61	124.63	188.52	5844
	55	22.31	127.36	183.02	5913
	65	23.18	130.02	176.41	6124
	75	24.53	136.74	169.04	6805
24% coverage	0	20.73	124.40	197.30	5495
	45	22.29	125.79	180.99	5694
	55	23.89	133.01	173.51	6283
	65	26.43	146.56	162.65	7456
	68	27.68	152.46	155.72	7935
	72	29.39	158.86	147.58	8599
	75	30.35	164.00	144.77	9145

TABLE 2. Resulting right ventricular hemodynamics from rotation studies for the baseline heart failure case (No VAD), 12.5, 18.2, and 24% device coverage areas.

	Angle (°)	EF (%)	PSP (mmHg)	ESV (mL)	SW (mmHg mL)
No VAD		43.91	44.32	63.50	1793
12.5% coverage	0	44.91	43.60	60.82	1765
	45	42.53	43.71	66.93	1744
	55	42.12	43.95	68.71	1745
	65	41.82	44.49	70.35	1794
	75	42.69	45.10	69.38	1864
18.2% coverage	0	44.99	43.65	60.74	1781
	45	41.86	43.86	68.94	1762
	55	41.58	44.48	70.47	1786
	65	42.22	45.26	69.92	1878
	75	45.09	46.17	64.27	2007
24% coverage	0	44.94	43.59	60.86	1757
	45	42.45	44.32	68.97	1745
	55	45.12	46.02	63.81	1900
	65	53.09	49.14	49.07	2193
	68	58.78	51.02	40.21	2357
	72	65.60	53.24	31.02	2561
	75	69.18	54.56	26.62	2673

higher afterload pressures (Fig. 5). Indeed, the highest angle of rotation tested here (75°) produced a 72% improvement in LV SW when compared to baseline. Interestingly, we also observed a stepwise decrease in ESV with increasing torsion angle in the LV, suggesting that AAT helps the ventricle to empty more completely during each cardiac cycle while also helping to unload the heart during the filling phase of the cardiac cycle (Fig. 6).

Apical CA also proved to be a key factor in optimizing tVAD performance in these simulations, albeit to a lesser degree than rotation angle. Nevertheless, as device coverage was increased from 12.5 to 24%, there was a consistent trend toward healthier cardiac hemodynamics. Though the effects of CA on cardiac function were relatively subtle, EF, PSP and SW all increased and ESV decreased with greater device coverage (Tables 1 and 2). This general pattern was maintained across all three CAs tested, with the most marked improvements found in simulations with the highest device coverage.

Furthermore, we noted a large increase in EF, PSP and SW in the numerical experiments with largest apical CA. However, a potential plateau in the
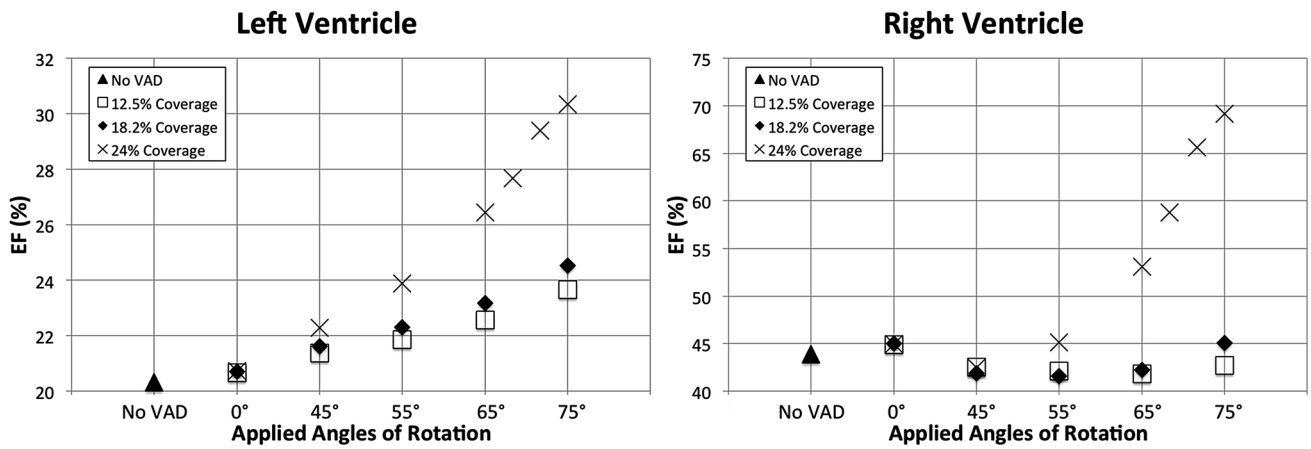
Left Ventricle

Right Ventricle

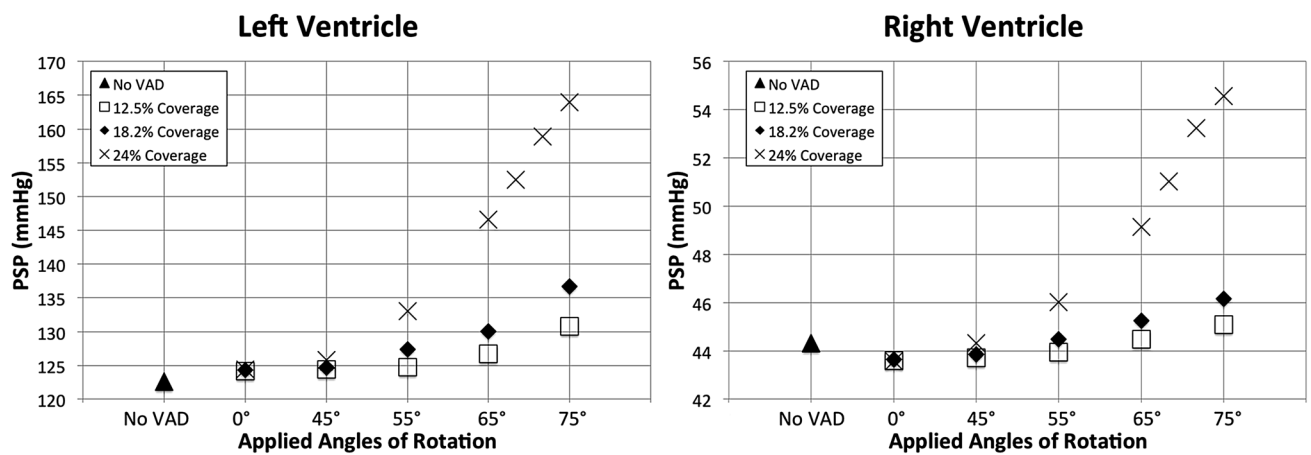FIGURE 3.   EF as a function of the applied angle of rotation and tVAD coverage in both left and right ventricles.

Left Ventricle

Right Ventricle

FIGURE 4.   PSP as a function of the applied angle of rotation and tVAD coverage in both left and right ventricles.

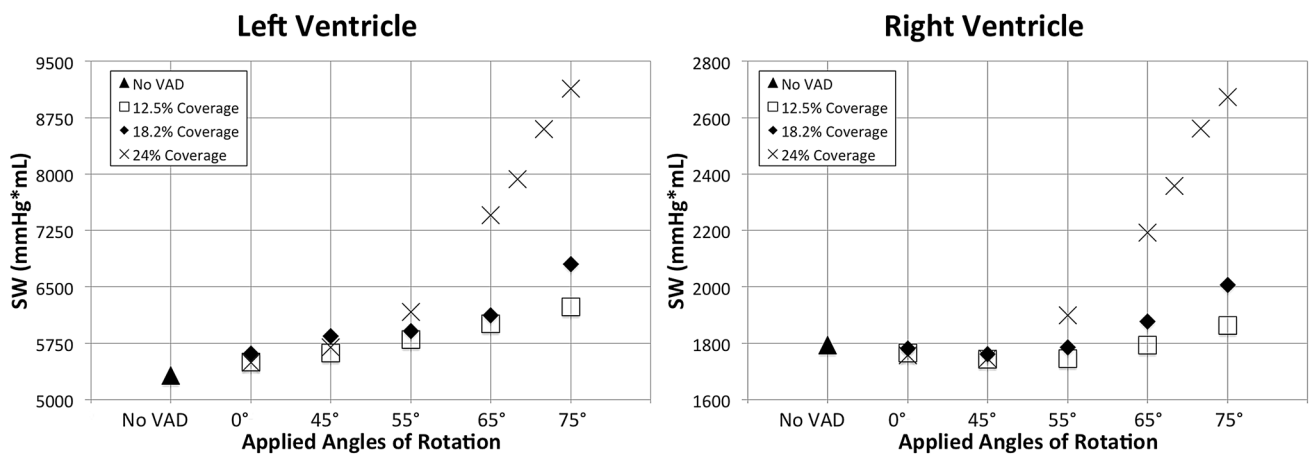## Left Ventricle

Right Ventricle

FIGURE 5.   SW as a function of the applied angle of rotation and tVAD coverage in both left and right ventricles.

hemodynamic parameters occurs between 65° and 75°. Two additional simulations at 68.33° and 71.67° were completed to investigate this phenomenon. The results were consistent with the previous simulations where an upward trend in EF, PSP, and SW and a downward trend in the ESV were noted.

LV and RV pressures were plotted as a function of their respective volumes at varying rotation angles as a
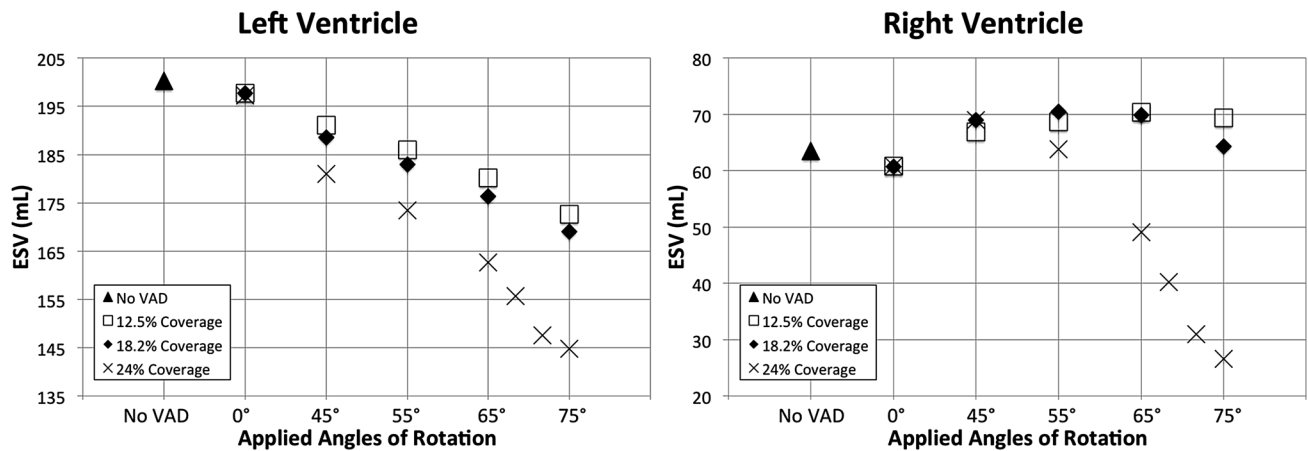
FIGURE 6. ESV as a function of the applied angle of rotation and tVAD coverage in both left and right ventricles.

means to visualize the effects of AAT on global cardiac mechanics (Figs. 7 and 8). As rotation angles were increased, the LV PV-loops became proportionally larger both in terms of pressure generation (vertical axis) and volume displacement (horizontal axis) when compared to the baseline clinical HF model. The widening of the PV-loops with increasing torsion angles suggests that tVAD actuation is effectively helping the ventricle to eject a greater volume of blood with every cardiac cycle, increasing CO proportionally. The lengthening of the PV-loops in the vertical direction with increasing torsion angles indicates that the tVAD is able to help generate higher arterial pressures by mechanically deforming the ventricular volume. And finally, the leftward shift of these loops indicates that AAT causes significant ventricular unloading, which may be beneficial as the heart remodels over time. These effects are more subtle for the RV (Fig. 8). The largest changes in the PV-loops occur for the two largest rotation angles (65° and 75°).

DISCUSSION

Cardiac assist devices have come a long way since their introduction 50 years ago.[26] In that time, the armamentarium of blood pumps available to clinicians has been greatly expanded and systematically refined to meet the cardiac support needs of more HF patients than ever before. In this sense VAD therapy can be—and should be—considered an enormous success, especially to the thousands of patients who have directly benefitted from this life-saving technology. Still, despite the many technological triumphs that have marked the developmental history of the 'artificial heart,' longstanding problems of blood activation and driveline infections remain largely unresolved in the setting of long-term cardiac support. Consequently,

most blood pumps today are used either to treat patients in cardiogenic shock (rescue) or as a bridge to cardiac transplantation rather than as permanent replacements for the human heart.

While driveline management has been a persistent problem for VAD patients over the years, the foremost impediment to long term cardiac support has been hematologic complications caused by two main factors: the inherent thrombogenic properties of synthetic blood contacting surfaces and the systemic bleeding complications associated with impeller-driven pumps. Because blood clots are a serious concern with any blood-contacting device—heart valves and coronary stents included—systemic anticoagulation is required for all VADs currently approved for clinical use. Unfortunately, rotary blood pumps, which comprise the vast majority of devices on the market today, make the use of these 'blood thinners' especially problematic since shear-induced proteolysis of von Willebrand factor can lead to serious bleeding problems elsewhere in the body. Pulsatile VADs tend to be gentler on the blood and cause fewer bleeding problems, but this advantage is largely mitigated by their having much larger blood contacting surfaces to manage. Consequently, thrombotic and bleeding complications remain a major source of morbidity and mortality among VAD patients to this day.[11] For these reasons we believe that non-blood-contacting assist schemes like the apical torsion approach described here may be especially well suited for patients requiring chronic circulatory support.

Previously, we demonstrated the potential of AAT as a therapy for CHF in a pilot study using a simplified version of our current working computational model.[28] In these preliminary simulations, an idealized, high-order, 18-element left ventricular prolate spheroidal model with both normal (54% EF) and reduced (31% EF) contractile function was subject to varying degrees
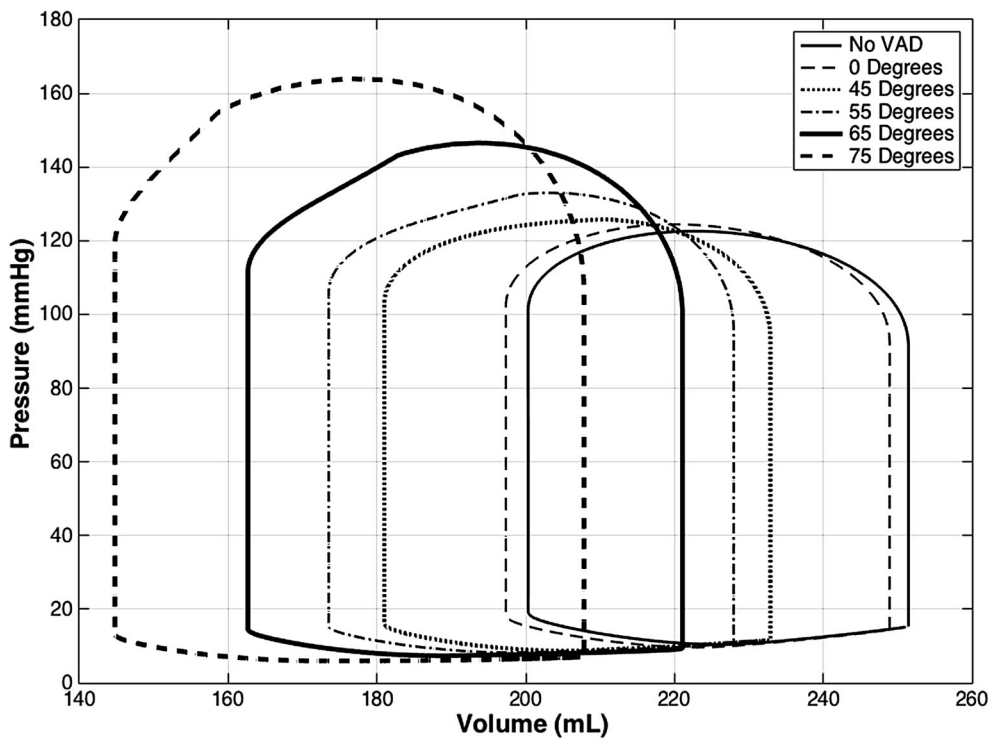
FIGURE 7. Left ventricular PV-Loops for a rotation study at the high (24%) coverage area.
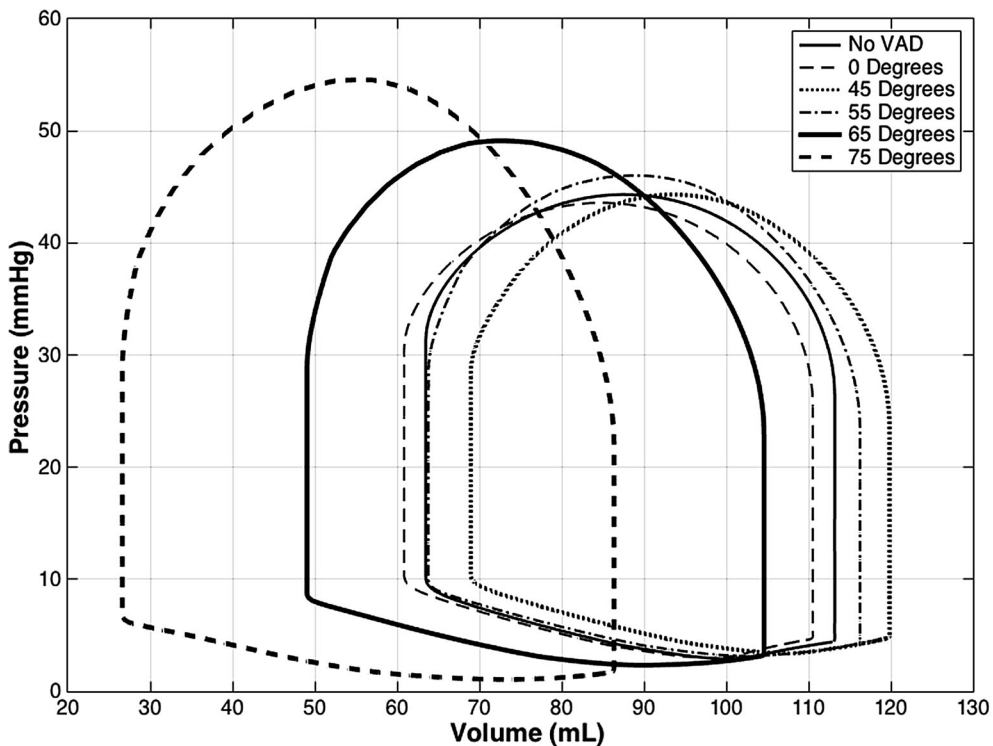

FIGURE 8. Right ventricular PV-Loops for a rotation study at the high (24%) coverage area.

of AAT during the systolic portion of the cardiac cycle. In these experiments the virtual torsion apparatus was designed to cover 22% of the distance from the apex to the base. Results from the reduced function model showed significant improvements in LV stroke volume and peak pressure generation of 9.9 and 11.7%

respectively at rotation angles of 90°. These results were found to be in substantial agreement with values recorded in experiments using a porcine model of acute HF wherein LV stroke volume increased by 17.1% and peak pressures rose by 10.9% under similar support conditions.

In this study we investigated the effects of AAT on the failing heart in more detail by conducting a series of parametric numerical experiments examining the effects of rotation angle and device CA using an advanced, biventricular model of a failing human heart. Results from these computational studies suggest that global hemodynamics of the failing heart can be significantly improved with AAT and that these improvements are a strong function of both rotation angle and device CA. Specifically, we found that EF, PSP and SW trended sharply upward with increasing angles of rotation and CA while ESV values were significantly reduced.

When compared to the baseline pretreatment HF condition, the most aggressive tVAD assist approach tested—i.e., 24% CA and 75° rotation—increased LV EF and SW production by 49 and 72%, respectively. These same torsion parameters also yielded significant gains in EF (58%) and SW (49%) on the right side, which bodes well for the prospect of using AAT for biventricular support. Increases in LV EF for the small and intermediate coverage cases were modest. But when combined with moderate increases in peak LV pressures, a moderate increase in SW occurs for small coverage and a substantial increase occurs for intermediate coverage (Table 1). Simultaneously, ESV diminishes substantially in both cases. For the large coverage case, the increases in EF and SW are dramatic, along with large reductions in ESV. Some other potential important findings are the large increases in SW for both ventricles between the 65° and 75° cases, particularly for the largest coverage (Tables 1 and 2). The hemodynamic improvements between 65° and 75° also seemed to plateau, especially with larger CAs. Extra simulations at 68.33° and 71.67° for the large CA were completed. We indeed confirmed that hemodynamics increased and decreased with a similar trend to the rest of the results, but the hemodynamic returns lessened as the rotation angle neared 75°. Based on these findings, we believe that assist for the large CA with ARA between 72° and 75° may be the optimal tVAD working parameters.

Our results from the first realistic biventricular simulations of AAT are very encouraging, and they raise some other issues and questions that can be addressed with additional simulations using versions of the existing computational model, including the following. The timing and duration of the applied rotation for all of our studies has been a sinusoidal systolic rotation that takes one-quarter of the cardiac cycle and a linear return rotation taking up the remainder of each cardiac cycle. However, reviewing the PV-loops (Figs. 7 and 8) shows that this timing may not be optimal, especially with regard to the LV loops with ARAs of 55° through 75°. It appears that ejection diminishes substantially at times considerably before isovolumic relaxation starts. Therefore, it may be possible to increase ejection with longer systolic rotations for these cases.

An effort to increase the coverage region to 36% failed, even for ARAs as low as 45°. One hypothesis that may explain these diverging solutions is described under the limitations section subsequently. However, it may be worthwhile to attempt 30% coverage with a modification of one of the existing models. Even if solutions can be obtained only for lower maximum ARAs, they may provide an upper limit on coverage (above 24%) that still yields substantial improvement in function without the more severe rotations. Finally, all of these studies were performed with models that produced baseline LV EFs of about 20%. But, EFs in HF are highly variable from patient to patient. Therefore, a parametric study in which baseline EFs are varied will be performed. This requires careful tuning of the dynamic model and/or the parameters of the circulatory model. In particular, it will be intriguing to determine whether or not considerably greater improvements in function can be achieved with applied rotation in HF cases that are even worse, with EFs at 15% or even 10%, as have been reported in the clinical literature.[2]

The ultimate goal of these follow-on experiments will be to guide the design of a clinically relevant tVAD interface and actuation mechanism that can be used to test and validate this approach on the bench top, in porcine HF models and, ultimately, in clinical CHF patients. For these simulations of a CHF heart model with a baseline EF of 20%, we have narrowed down an optimal set of working parameters, especially at the large CA. It is foreseeable to improve hemodynamic returns at lower CAs by further investigating the other methods mentioned, e.g., adjusting the timing or varying the functions of the applied rotation. Beyond this, further studies will be needed to understand the resulting stresses and strains that the heart experiences as these torsional deformations are imposed on the myocardium. Furthermore, studies are needed to examine the effects of varying modes of HF and cardiac disease states, e.g., varying levels of ventricular dilation, right ventricular failure, cardiac hypertension and myocardial infarction. The final task to be accomplished prior to *in vivo* device testing will be to develop a method to securely attach the tVAD to the epicardial surface of the heart. The challenge here will

be to design an attachment scheme that will provide secure fixation of the device to the smooth, slick surface of the heart while causing minimal damage to the epicardium.

Study Limitations

Although there are numerous advantages to using a computational model to quantify the effects of AAT on the beating heart, the limitations of this study fall mainly on the assumptions of the model itself. In these computational experiments we have addressed the fundamental limitations of our first computational study by replacing the 18-element simplified pig prolate spheroidal model with a more realistic biventricular model based on measurements from a clinical patient with dilated cardiomyopathy. By adopting this advanced beating heart computer model, results from these simulations are far more realistic than those reported earlier. At the same time however, the computational complexity of this model and its realistic replication of a failing human heart result in much longer simulation run times. This makes comprehensive parametric studies of the sort needed to thoroughly characterize tVAD performance under a wide range of clinical conditions difficult, expensive and time consuming. The simulations with increasing values of maximum ARA take considerably longer to converge than our typical baseline simulations of HF. One hypothesis that may explain this phenomenon is an interaction between active state and the applied rotation. Fortunately, the finding that the use of the final conditions for a run involving a smaller angle as the starting point for a subsequent run with a larger angle obviates this difficulty somewhat. Also, it is important to note that while simulations of this sort provide important information regarding the biomechanics of AAT that would be difficult or impossible to obtain experimentally, they cannot determine the biological effects of tissue/device interactions or predict damage that might occur at the cellular level with the cyclic application of torsional stress across the ventricular walls.

Indeed, though the improvements in global cardiac hemodynamics reported here are very promising, the extent to which this artificial wringing of the heart is likely to injure the myocardium, damage the epicardial surface, compromise valve function, or interfere with normal sinus rhythm remains an open question. In our previous study we found that acute application of the tVAD did not generate any visible damage to the beating heart or induce any noticeable adverse cardiac events.[28] However, the long-term effects of applied torsion on the overall health of the heart can only be inferred from forthcoming computational analyses in which myocardial finite strains, accompanying stresses and force resultants, particularly in the neighborhood of the mitral annulus, are estimated. And, they must be confirmed via chronic implant trials.

Potential Advantages of tVAD Support

These multi-scale simulation studies strongly suggest that, from a purely biomechanical standpoint, AAT has the potential to be an effective means to support the failing heart without the problems of thrombolysis and blood activation common to all blood contacting cardiac assist devices. As such, this approach would effectively eliminate the need for anticoagulation and avoid long-standing blood handling complications that have largely limited VAD use to rescue and bridge-to-transplant applications. Also, because of its positioning at the apex of the heart with contact surfaces extending up the walls of both ventricles, the tVAD has the potential to provide true biventricular support, whereas most clinical devices currently on the market address left HF alone. This is an important distinction because, while some patients who present with biventricular failure can show improvement in right heart function with left heart support, there are far fewer options available for patients with true biventricular HF. The tVAD could be used, in principle, to treat this underserved patient population.

Another potential benefit of this approach stems from the fact that the tVAD works by extending the natural twisting motion of the heart to improve ventricular ejection. This singular mechanism may provide a means to unload the ventricles while allowing the myocardium to continue to contract, which could conceivably promote cardiac recovery over time. Should the heart respond to chronic tVAD therapy by gradually regaining contractile function, the patient could be weaned easily from the device by systematically lowering the level of rotational assist to provide the minimum level of support needed. If myocardial reverse remodeling were to advance to the point where normal cardiac function was fully restored, the device could either be removed entirely or deactivated *in situ* to retain the option of further support should the need arise.

APPENDIX 1

More details of the computational modeling methods are provided here including the passive material properties, parameters of the cellular model used to simulate active state, the initial conditions and parameters of the dual, closed-loop circulatory models,

boundary conditions, selected aspects of model geometry, and data analysis.

ContinuityPro Simulation—Additional Notes

The model used in CRT studies had only 48 elements, and the circumference at 12.5% already existed from the original construction of the model. Each new circumference adds 16 tri-cubic elements. In these studies, a regular refinement of the most apical set of elements in the longitudinal direction was performed. This provided a circumference between 12.5% and the apex yielding additional nodes for applied rotation. Then, an irregular refinement of the elements between 12.5% and the equator of the model was performed to provide a circumference at 24%. This was done by trial-and-error to obtain 24.0% coverage with precision, and yielded an 80-element model used in much of this research. An effort was made to add an additional circumference precisely at 36% coverage, so that coverage of 12.5, 24 and 36% would be available. However, this model fails to converge in reasonable time steps, even for the peak rotation angle of 45°. Potential reasons for this difficulty are described in the discussion. Therefore, to provide an intermediate coverage

model, a regular refinement was performed between 12.5 and 24% yielding 18.2% coverage and the concomitant potential to study 3 coverage cases. The intermediate coverage model has 96 elements.

Two versions of the same finite element model were employed to make overall solution times for the parametric studies more practical. The models are identical in every way, except for the amount of refinement. For the smallest and largest CAs, an 80-element tri-cubic Hermite model was employed. For the intermediate CA, the 96-element model with one additional circumference midway between smallest and largest CAs was used (Fig. 1). To verify the accuracy of the 80-element model, the larger model was rerun for the largest rotation (75°), the most challenging case, with small and large CAs. Results for small coverage were different between the two models by 1% or less. Those for large coverage were different by 4% or less.

The CircAdapt model[1] used to simulate the circulations in the CRT studies[16] is not available in Continuity Pro. Moreover, several substantial modifications had to be made to Continuity Pro to make the moving boundary problem possible. These changes have not been made to the academic version, Continuity, so that the current studies cannot be performed using that software at this time. Instead, the two-chamber finite element model is connected to lumped parameter closed-loop circulatory systems that account for the atria as well as the systemic and pulmonic circulations.[15]

When varying the ARA for a given CA, a second, effective method that yields the same results can be used. Rather than run simulations for 10 or more cycles for each ARA after inflation, the 55° case can be

TABLE 3. Parameters of nonlinear, transversely isotropic material law.

Passive constitutive law	Parameters
Stress scaling coefficient (kPa)	0.80
Fiber strain coefficient	18.50
Transverse strain coefficient	3.58
Fiber-transverse shear coefficient	1.63
Bulk modulus	500.00

TABLE 4. Parameters of cellular model used to simulate active state.

Dynamic cellular model	Parameters
Unloaded sarcomere length (μm)	1.95
Active stress scaling parameter (kPa)	0.95
Intracellular calcium concentration ($\mu mol/L$)	4.35
Maximum isometric tension (kPa) at longest sarcomere length	100.00
Length-dependent calcium sensitivity constant (kPa)	1.80
Sarcomere length at which active force is zero (μm)	1.58
Maximum peak intracellular calcium concentration ($\mu mol/mL$)	4.35
Hill coefficient in calcium sensitivity	2.00
Slope of relation between time-to-peak tension and sarcomere length (ms/μm)	52.49
Intercept of relation between time-to-peak tension and sarcomere length (ms)	55.26
Slope of relation between relaxation duration and sarcomere length (ms/μm)	131.20
Intercept of relation between relaxation duration and sarcomere length (ms)	−94.34
Twitch duration scaling factor	1.4625
Cardiac cycle duration (ms)	750.00

TABLE 5. Parameters and initial conditions of circulatory models.

Closed loop with atria for LV and RV: systemic and pulmonic circulations	Parameters
Left ventricular pressure-initial condition (kPa)	1.50
Right ventricular pressure-initial condition (kPa)	1.00
Volume of left atrium-initial condition (mL)	37.33
Volume of systemic vessel 1-initial condition (mL)	440.00
Volume of systemic vessel 2-initial condition (mL)	1800.00
Volume of right atrium-initial condition (mL)	35.00
Volume of pulmonic vessel 1-initial condition (mL)	225.00
Volume of pulmonic vessel 2-initial condition (mL)	120.00
Right atrium maximum elastance (kPa/mL)	0.03
Right atrium minimum elastance (kPa/mL)	0.0273
Right atrium unloaded diastolic volume (mL)	14.00
Right atrium unloaded systolic volume (mL)	13.00
Tricuspic valve resistance (kPa-ms/mL)	0.50
Arterial impedance (right) (kPa-ms/mL)	4.00
Compliance of vessel 1-right (mL/kPa)	60.00
Resistance of vessel 1-right (kPa-ms/mL)	21.00
Volume of vessel at zero pressure-right (mL)	0.00
Compliance of vessel 2-right (mL/kPa)	65.00
Resistance of vessel 2-right (kPa-ms/mL)	4.00
Volume of vessel 2 at zero pressure-right (mL)	0.00
External pressure-right (kPa)	0.00
Basic cycle length-left (ms)	750.00
Time of atrial activation-left (ms)	100.00
Atrial twitch duration-left (ms)	375.00
Left atrium maximum elastance (kPa/mL)	0.7823
Left atrium minimum elastance (kPa/mL)	0.0711
Left atrium unloaded diastolic volume (mL)	14.00
Left atrium unloaded systolic volume (mL)	13.00
Mitral valve resistance (kPa-ms/mL)	0.50
Arterial impedance-left (kPa-ms/mL)	7.00
Compliance of vessel 1-left (mL/kPa)	32.60
Resistance of vessel 1-left (kPa-ms/mL)	126.00
Volume of vessel 1 at zero pressure left (mL)	0.00
Compliance of vessel 2-left (mL/kPa)	433.00
Resistance of vessel 2-left (kPa-ms/mL)	51.40
Volume of vessel 2 at zero pressure (mL)	0.00
External pressure-left (kPa)	0.00
Number of pressure estimations (settings)	10.00
Total number of time steps (settings)	20,000.00
Relative volume accuracy (settings)	0.0001

simulated by starting from the final conditions of the 45° run. The final configuration and final circulatory state variables at the last end-diastolic state of the 45° run provide the starting point (initial conditions) for the 55° simulation. This method provides fully converged solutions much more quickly than simulations that start from the initial inflated state. Then, the 65° case can be run starting at the endpoint of the 55° run, and so forth.

A consistent finding has been that a failure to converge with this time step is not necessarily obviated with smaller time steps; and simulations using half millisecond time steps take as long as two days to solve regardless of the number of parallel cores due to the current parallelization scheme for the biomechanics

module of Continuity Pro (and its progenitor, the academic version of Continuity at UCSD).

Passive Properties

The material law used in the CRT studies[13] is accurate in estimating normal and pathophysiologic cardiac function. However, it no longer applies for very large deformations, as induced in the current simulations. As the bulk modulus is raised, the elements are no longer isochoric and deviate substantially from values of J (det $\mathbf{F}$) close to unity, as the authors describe.

Therefore, another nonlinear, transversely isotropic material law was used to simulate the passive proper-
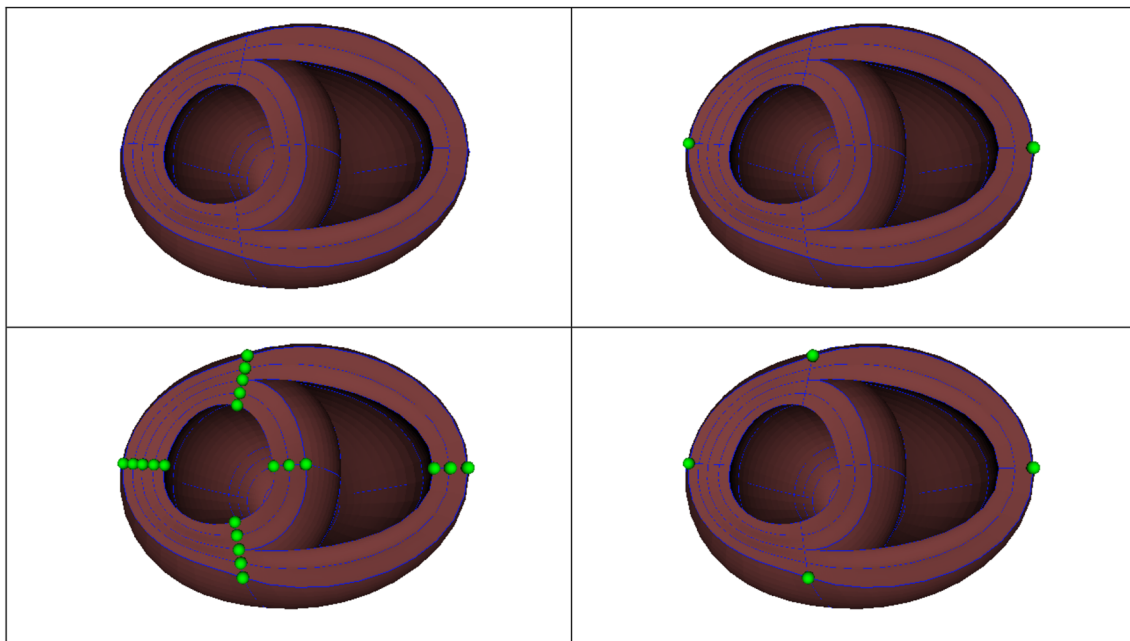
FIGURE 9. Fixed boundary conditions on the base of the model are shown; base of the model (upper left); two epicardial nodes fixed in l (upper right); all basal nodes fixed in m (lower left); four epicardial nodes fixed in q (lower right).

TABLE 6. Cavity volumes as a function of applied rotation angle in the LV.

Cavity volumes in selected angles-LV				
State angles (°)	65.00	68.33	71.67	75.00
No load (mL)	134.8	134.8	134.8	134.8
End-diastole-large coverage (mL)	221.1	215.3	209.0	207.8
Peak pressure-large coverage (mL)	194.1	185.0	179.4	176.3
End-systole-large coverage (mL)	162.6	155.7	147.6	144.8

TABLE 7. Cavity volumes as a function of applied rotation angle in the RV.

Cavity volumes in selected angles-RV				
State (°)	65.00	68.33	71.67	75.00
No load (mL)	70.4	70.4	70.4	70.4
End-diastole-large coverage (mL)	104.6	97.5	90.2	86.3
Peak pressure-large coverage (mL)	72.7	64.9	59.0	55.2
End-systole-large coverage (mL)	49.1	40.2	31.0	26.6

ties of the ventricles. This constitutive law allows for increases in the bulk modulus to ensure that J remains close to unity. It is a modified version of the law described earlier[12] that is defined in terms of a hyperelastic, exponential strain energy function. A slightly compressible version was developed that provides better convergence characteristics than an incompressible version using standard Lagrange multiplier/ penalty function techniques. This version was improved further with a more advanced version of the compressible term.[7] For typical heart simulations, this material law provides accurate results with a bulk modulus of 350, including normal and pathophysiologic function. However, for the current studies, it was necessary to raise the bulk modulus to 500 in order to maintain isochoric elements throughout the cardiac

cycles due to very large myocardial deformations induced by the applied rotations, particularly at the largest angles during systole (Table 3).

Dynamic Properties: Cellular Modeling

The cellular model used to simulate active state is a modified Hill-type model with length-dependent activation that was used in our previous research on single ventricle tVAD simulation. It was first developed earlier.[30] The parameters used in these studies are listed in Table 4. These values reduce contractility and are used in conjunction with abnormal circulatory parameters to simulate baseline heart failure. The passive and dynamic properties listed here are constant throughout these studies.

Circulatory Properties

The dual circulatory models with atria are based on earlier research in which stable closed-loop systems were developed[15] The initial conditions and parameters of the pulmonic and systemic circulatory systems are shown in Table 5. The parameters were based on an extensive review of the heart failure literature and reflected expected increases in arterial impedances and resistances and decreased arterial compliances.[4–6,8–10,12,14,17–22,25,29] Final adjustment of these parameters in test runs yielded an LVEF of about 20% in the pretreatment state.

Boundary Conditions

Fixed boundary conditions at the base of the model are shown in Fig. 9.

Biventricular Geometry

The dimensions of the model in the no load state are 12.1 cm from the epicardium of one free wall to that of the opposite free wall at the equator, 9.3 cm orthogonal to the first dimension, 8.1 cm from the left free wall epicardium to the RV septum (endocardium) and 9.3 cm in the longitudinal direction from base to apex.

Selected left- and right-ventricular cavity volumes are provided in Tables 6 and 7. Cavity volumes for the large coverage case undergoing applied rotations at 65°, 68.33°, 71.67° and 75° are shown. Pressure–volume loops for all cases are given in the results section.

Stroke Work Analysis

To calculate SW, Image J (U.S. National Institutes of Health, Bethesda, Maryland, USA) was used to measure the area circumscribed by the PV-loop of that cardiac cycle. This method is considerably easier than using MatLab for the same purpose and just as accurate. When using the latter, it is necessary to perform two integrations using the trapz function for nonuniform grids. It is also vital to consider precise outflow valve openings and closings to isolate the ejection curves and inflow valve openings and closings to isolate the filling curves. But, this is unnecessary when Image J is used to get the entire area of each PV-loop with a single click of the Wand tool and use of the Measure function. It is important to calibrate the results to obtain SW in units of mmHg mL. Accurate calibrations are performed using the largest rectangle available on the plot. When done properly, Image J gives virtually identical results to the more cumbersome use of MatLab for this purpose. In the case of the largest rotation and largest CA, results from Matlab were compared with Image J. They were virtually identical, 9145 mmHg mL using Image J and 9171 mmHg mL using MatLab, a difference of less than 0.3%.

CONFLICT OF INTEREST

The authors declare that they have no conflict of interest.

REFERENCES

[1]Arts, T., T. Delhaas, P. Bovendeerd, X. Verbeek, and F. Prinzen. Adaptation to mechanical load determines shape and properties of heart and circulation: the CircAdapt model. *Am J Physiol Heart Circ Physiol* 288(4):H1943–H1954, 2005.

[2]Ashley, E. A., Niebauer, J. Heart failure. In: Cardiology Explained, edited by T. Berthoud, H. James, R. O'Brien, and C. Harris. London: Remedica, 2004, p. 100.

[3]Centers for Disease Control and Prevention. Heart Failure Fact Sheet. Atlanta: Centers for Disease Control and Prevention, 2013.

[4]Chemla, Denis, Jean-Louis Hébert, Catherine Coirault, Karen Zamani, Isabelle Suard, Patrice Colin, and Yves Lecarpentier. Total arterial compliance estimated by stroke volume-to-aortic pulse pressure ratio in humans. *Am J Physiol Heart Circ Physiol* 274(2):H500–H505, 1998.

[5]Dabestani, Ali, Gregory Mahan, Julius M. Gardin, Katsu Takenaka, Cora Burn, Alice Allfie, and Walter L. Henry. Evaluation of pulmonary artery pressure and resistance by pulsed doppler echocardiography. *Am J Cardiol* 59(6):662–668, 1987.

[6]Del Río, M., Liotta, D., Cervino, C.O. Vascular resistance and vascular impedance. In: A Practical Textbook of Congenital and Acquired Diseases of the Aorta, edited by D. Liotta. Buenos Aires: University of MoRón, 2003, pp. 52–53.

[7]Doll, S., and K. Schweizerhof. On the development of volumetric strain energy functions. *J Appl Mech* 67(1):17–21, 1999.

[8]Finkelstein, S. M., J. N. Cohn, V. R. Collins, P. F. Carlyle, and W. J. Shelley. Vascular hemodynamic impedance in congestive heart failure. *Am J Cardiol* 55(4):423–427, 1985.

[9]Freis, E. D., H. W. Schnaper, R. L. Johnson, and G. E. Schreiner. Hemodynamic alterations in acute myocardial infarction. I. Cardiac output, mean arterial pressure, total peripheral resistance, central and total blood volumes, venous pressure and average circulation time 12. *J Clin Invest* 31(2):131–140, 1952.

[10]Gamble, G., J. Zorn, G. Sanders, S. Macmahon, and N. Sharpe. Estimation of arterial stiffness, compliance, and distensibility from M-Mode ultrasound measurements of the common carotid artery. *Stroke* 25(1):11–16, 1994.

[11]Givertz, M. M. Ventricular assist devices: important information for patients and families. *Circulation* 124:e305–e311, 2011.

[12]Guccione, J. M., A. D. McCulloch, and L. K. Waldman. Passive material properties of intact ventricular myocardium determined from a cylindrical model. *J Biomech Eng Trans* 113:42–55, 1991.

[13]Holzapfel, G., and R. Ogden. Constitutive modeling of passive myocardium: a structurally based framework for material characterization. *Philos Trans R Soc A* 367:3445–3475, 2009.

[14]Kerckhoffs, R. C. P. Patient-specific modeling of the cardiovascular system: technology-driven personalized medicine. New York: Springer Science & Business Media, 2010.

[15]Kerckhoffs, R. C. P., M. Neal, Q. Gu, J. B. B. Bassingthwaighte, J. H. Omens, and A. D. McCulloch. Coupling of a three-dimensional finite element model of cardiac ventricular mechanics to lumped systems models of the systemic and pulmonic circulation. *Ann Biomed Eng* 35:1–18, 2007; (PMCID: 2872168).

[16]Krishnamurthy, A., C. T. Villongco, J. Chuang, L. R. Frank, V. Nigam, E. Belezzuoli, P. Stark, D. E. Krummen, S. Narayan, J. H. Omens, A. D. McCulloch, and R. C. P. Kerckhoffs. Patient- specific models of cardiac biomechanics. *J Comput Physics* 244:4–21, 2013. doi:10.1016/j.jcp.2012.09.015; (PMCID: 3667962).

[17]Lehmann, E. D., K. D. Hopkins, A. Rawesh, R. C. Joseph, K. Kongola, S. W. Coppack, and R. G. Gosling. Relation between number of cardiovascular risk factors/events and noninvasive doppler ultrasound assessments of aortic compliance. *Hypertension* 32(3):565–569, 1998.

[18]Liu, Z. R., C. T. Ting, S. X. Zhu, and F. C. Yin. Aortic compliance in human hypertension. *Hypertension* 14(2):129–136, 1989.

[19]London, G. M., M. E. Safar, A. C. Simon, J. M. Alexandre, J. A. Levenson, and Y. A. Weiss. Total effective compliance, cardiac output and fluid volumes in essential hypertension. *Circulation* 57(5):995–1000, 1978.

[20]Murgo, J. P., N. Westerhof, J. P. Giolma, and S. A. Altobelli. Effects of exercise on aortic input impedance and pressure wave forms in normal humans. *Circ Res* 48(3):334–343, 1981.

[21]Normal Hemodynamic Parameters and Laboratory Values. Irvine: Edwards Lifesciences LLC, 2009.

[22]O'rourke, M. F., J. A. Staessen, C. Vlachopoulos, D. Duprez, and G. E. E. Plante. Clinical applications of arterial stiffness: definitions and reference values. *Am J Hypertens* 15:426–444, 2002.

[23]Roche, E.T., M.A. Horvath, Alazmani, A, et al. Design and fabrication of a soft robotic direct cardiac compression device. In: ASME. International Design Engineering Technical Conferences and Computers and Information in Engineering Conference, Volume 5A: 39th Mechanisms and Robotics Conference, V05AT08A042, 2015. doi:10.1115/DETC2015-47355.

[24]Soohoo, E., H. Ma, A. Alcasid, and D. R. Trumble. Torsional ventricular assist device (tVAD): design considerations and prototype development. *J Med Dev* 2016. doi:10.1115/1.4033117.

[25]Tanaka, H., F. A. Dinenno, K. D. Monahan, C. M. Clevenger, C. A. Desouza, and D. R. Seals. Aging, habitual exercise, and dynamic arterial compliance. *Circulation* 102(11):1270–1275, 2000.

[26]Texas Heart Institute. Heart Assist Devices—Texas Heart Institute. Houston: Texas Heart Institute, 2016.

[27]Mayo Clinic Staff. Heart Failure. Treatments and Drugs. Mayo Clinic, 2016.

[28]Trumble, D. R., W. McGregor, R. C. P. Kerckhoffs, and L. K. Waldman. Cardiac assist with a twist: apical torsion as a means to improve heart function. *J Biomech Eng* 133:101003, 2011. doi:10.1115/1.4005169.

[29]Usyk, T. P., R. Mazhari, and A. D. McCulloch. Effect of laminar orthotropic myofiber architecture on regional stress and strain in the canine left ventricle. *J Elast* 61:143–164, 2000.

[30]Walker, J. C., M. B. Ratcliffe, P. Zhang, A. W. Wallace, B. Fata, E. W. Hsu, D. Saloner, and J. M. Guccione. MRI-based finite-element analysis of left ventricular aneurysm. *Am J Physiol Heart Circ Physiol* 289:H692–H700, 2005.